POLITECNICO DI TORINO
Repository ISTITUZIONALE

Live Wire - A Low-Complexity Body Channel Communication System for Landmark Identification

(Article begins on next page)

25 April 2024

Live Wire – A Low-Complexity Body Channel Communication System for Landmark Identification

Marco Crepaldi[1], Alessandro Barcellona[1], Giorgio Zini[1], Alberto Ansaldo[2], Paolo Motto Ros[3], Alessandro Sanginario[3], Claudia Cuccu[3], Danilo Demarchi[3] and Luca Brayda[4]

Abstract— **This paper presents a robust simplex Body Channel Communication (BCC) system aimed at providing an interactive infrastructure solution for visually impaired people. Compared to existing BCC solutions, it provides high versatility, wearability and installability in an environment in a low complexity hardware-software solution. It operates with a ground referred– transmitter (TX) and it is based on an asynchronous threshold receiver (RX) architecture. Synchronization, demodulation and packetizing and threshold control are completely software defined and implemented using MicroPython. The RX includes Bluetooth® (BT) radio connectivity and a cell-phone application provides push text-to-speech notifications to a smartphone. The hardware achieves a Packet Error Rate (PER) of ∼0.1 at 550 kHz pulse center frequency, Synchronized-On Off Keying (S-OOK) modulation and 1 kbps data rate, for an average current consumption of 44 mA.**

Index Terms— **Body Channel Communication, Interactive Infrastructure, MicroPython.**

I. INTRODUCTION

Body Channel Communication (BCC) can be interpreted as the exchanging of information through a movable, living and self-contained transmission medium, that is, the human body. The original and main application idea behind BCC is to enable the private information exchange among wearable nodes placed on the human body, optionally connected to another portable concentrator operating as a gateway for the cloud or simple internet infrastructure connections [1]–[3]. Recent research trends, however, show an increased interest in the exploitation of BCC systems to enable interactive infrastructure communication [4]–[6]. This human-to-environment extension has led to the design of systems with diverse configurations in terms of electrodes placement both on- and off-body [7], [8]. Thanks to BCC, space can be interactively explored as a person must touch the surrounding objects to gather information.

The above aspect is paramount in applications for visually impaired people, who regularly seek for information with an active limb motion. This is a substantially different way of interacting with the environment compared to RFID [9], Beacon [10], and Impulse Radio Ultra-Wide Band (IR-UWB) [11] because these systems trigger interactions with humans regardless of physical haptic contact with the external world. Previous works introduced the concept of Capacitive Near-Field Communication (CapNFC) where capacitive communication can be used to enable ubiquitous interaction with objects in short-range spatial contexts [12]. However, CapNFC has been developed so that the user human body takes part in the transmission but it is not the final information recipient. Our research targets the implementation of a low-cost and low-complexity BCC system suitable for such human-to-environment extension, with awareness on the current consumer market trends (see, e.g., [13]) that include voice-assistance and integration in smart homes. Our solution, *Live Wire* (see preliminary results in [14]), is a kHz-range threshold-based impulse-radio non-coherent system (simplex TX-to-RX link) that solves the problem of co-locating haptic interaction with an object and the reception of digital information. It is intended to be implemented using low cost components, full programmability and the highest *installability* in the environment. *Live Wire* takes advantage of the low-frequency electric field approximation of the human body (quasi-static near-field) and at the same time of the ground connection of the TX. Owing to its features, the TX can be installed on any conductive object in the environment with ideally any possible shape, and it operates with a very low current. Being the TX directly connected to the reference voltage (ground), when the TX is touched, the human body acts as a wire by providing the signal at almost the same level throughout the body, therefore enabling both a high-impedance pick-up and a constant Signal-to-Noise Ratio (SNR), almost independent from the RX positioning. Moreover, the RX does not need to be in contact with the skin.

To counterbalance the human body electrical features variability, BCC devices encompass the use of tunable inductors to implement resonance w.r.t. coupling capacitance [15], [16]. In these cases an SNR enhancement is necessary as in capacitive BCC one out of two electrodes (both for TX and RX) are floating and the other is in contact with the skin and positioned vertically or horizontally w.r.t. the human body [17]. While this requirement normally impacts on system complexity, in *Live Wire* given the enforced low-impedance path to ground at the TX, the SNR remains constant throughout the body. Adaptativity, instead, is here translated into a front-end dynamic threshold adjustment to counterbalance environmental interference. Consequently an automatic gain control unit (AGC), see e.g. [18], is not required.

M. Crepaldi, A. Barcellona and G. Zini are with 1) the Istituto Italiano di Tecnologia (IIT) − Electronic Design Laboratory (EDL), Via Melen 83, 16152 Genova (GE), Italy, e-mail: marco.crepaldi@iit.it. A. Ansaldo is with 2) the Istituto Italiano di Tecnologia (IIT) − Graphene Labs, Via Morego 30, 16163 Genova (GE), Italy. P. Motto Ros, A. Sanginario, C. Cuccu and D. Demarchi are with 3) the Politecnico di Torino, Department of Electronics and Telecommunications, C.so Castelfidardo 39, 10129 Torino (TO), Italy. L. Brayda is with 4) the Istituto Italiano di Tecnologia (IIT) − Robotics Brain and Cognitive Sciences (RBCS), Via Melen 83, 16152 Genova (GE), Italy.
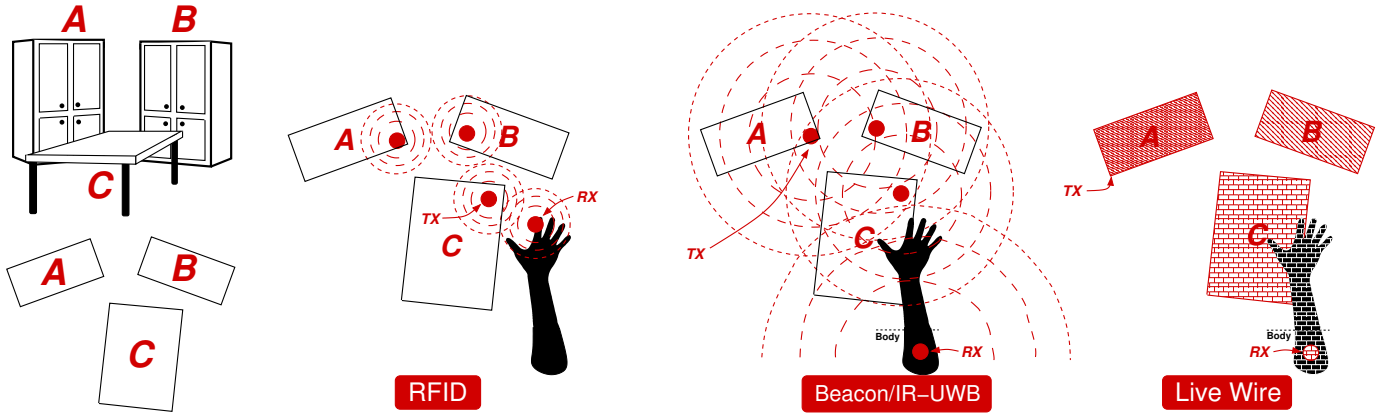
Fig. 1. Comparison between the RFID, Bluetooth® low energy Beacon/IR-UWB and *Live Wire* (BCC) technology.

Live Wire requires just a microcontroller I/O pin to drive the TX signal and a low-complexity front-end detector at the RX based on very limited number of external active components. Moreover, it is fully implemented using MicroPython (*μ*Py), an open source and easily extensible high-level programming language, increasingly used in real-time system development (see [19] and research in [20]) and considered as an interesting alternative to empower embedded systems [21]. Our contribution regards i) an innovative application to increase quality of life of visually impaired people, ii) an HW/SW architecture for landmarks exploration in smart environments, iii) an associated threshold control algorithm, iv) a working prototype including an experimental validation of the system. The paper is organized as follows: Sec. II details the application domain, Sec. III discusses the system architecture, and Sec. IV–V detail TX and RX prototype, the RX threshold adjustment algorithm, the RX internal firmware. Sec. VI presents detailed performance measurement results and functional validation obtained by installing the TX in different furniture, simply grounded though an USB port, and concludes with a state-of-the art comparison.

II. MOTIVATION AND APPLICABILITY

The application of the *Live Wire* technology is the identification of landmarks for visually impaired persons. *Live Wire*, unlike current approaches such as RFID and BT low-energy Beacon, is designed to allow a person without vision to seamlessly obtain digital information from common objects only by touching any part of them. The identification of landmarks is crucial because it is at the foundation of blind persons orientation and mobility strategies [22]. Without correctly identifying landmarks, navigation for blind persons is either too difficult or it must entirely rely on guides or technological aids, thus preventing the learning from the environment and implying relevant safety concerns. The literature is populated with Electronic Travel Aids (ETA) that very often increase the cognitive load of the landmark identification process, something known as the "masking phenomenon" [23]. Even if there is a large literature of indoor navigation systems (see [24] for a review), most studies focus on assisted navigation and only a few works consider that navigation is already a well-

trained process in blind persons, but landmark identification is not. Usually, blind persons identify large objects (furniture, home appliances) by means of Braille tags [25]. Due to their very small size compared with the object surface, they have to be found by an extensive tactile exploration, thus resulting uncomfortable, they cannot contain extensive information and cannot be tailored to user needs.

Fig. 1 compares three technological solutions to this problem, i.e., RFID, Beacon/IR-UWB and *Live Wire*. Here, three possible objects, i.e., closets A and B, and desktop C have to be unambiguously identified by the arm of a blind person. RFID has the advantage of deploying passive transmitters on any object, but it is known to have a limited radiation pattern. This forces the end-user to wear the transceiver in distal parts of the body (e.g. the closest to the hand) and to search for the RFID tag as in the Braille tag case, but without the advantage of explicit tactile feedback (RFID tags are not necessarily in relief). Beacons provide extended range, but crosstalk can make object pinpointing complicated. Importantly, with beacons the ecologic process of landmark identification, usually achieved with active haptic exploration, is completely decoupled from reception of data from the beacons. However, unlike RFID, Beacon allows wearing the receiver in any body part. *Live Wire*, instead, collects the advantages of their predecessors, without being limited by their drawbacks: *Live Wire* sends information from objects *only* if they are touched; it has the advantage of extending the range of information to the whole surface of an object without the disadvantage of crosstalk.

IR-UWB, similarly to Beacon, can enable location but more precisely. However, its performance strongly depends on Line-of-Sight (LOS) or Non-Line-Of-Sight (NLOS) conditions. Even in the best accuracy condition of ± 10 cm in LOS [11] accuracy is not sufficient, and the transceiver must be in close proximity with the object to be approached (with anchor nodes disseminated in the environment). A key point of *Live Wire*, instead, is that digital information is confined to the same haptic enclosure, therefore avoiding confusion between objects and preventing false alarms: digital information is co-located with haptic exploration. Moreover, the *Live Wire* RX can be worn anywhere on the body, e.g. inside cloths, therefore allowing interaction with hands, arms, legs. We expect that

blind persons using *Live Wire* would find natural to learn landmarks, since the process of identification is triggered by haptic exploration and enriched, for example, with audio information (e.g. "this is the closet with winter clothes" or "this shelf hosts biscuits and sweets" or "the table you are touching is at the center of the room").

III. LIVE WIRE BCC

A. High-Level Constraints

In commercial solutions such as BodyCom [26] transmission is based on a resonant LC load and base station (fixed node) and mobile device (wearable node) is initiated thanks to a capacitive touch detection on a pad electrode. The center frequency utilized for bidirectional communication is 125 kHz, that exploits the high permittivity of the human body which permits low-complexity transmission in the 60 kHz–10 MHz frequency range. However, due to capacitive/proximity detection and LC resonance, the pad needs to be carefully designed, which is totally in contrast with our application domain in which the user must have the freedom to touch any (metallic) part of the object in the infrastructure.

For applications involving able-bodied persons, the typical latency of human perception is 150 ms [27], while in other specific BCC implementation latency is considered in the range $10 - 250$ ms [28]. In general, these latency constraints can be applied to visually impaired people as well, as for these subjects the only difference is in the sensory modality with which information is received. However, the above bounds are valid in a real-time application in which latency is considered as a direct player in a closed perception/actuation loop (for instance drag and drop actions in touch-screens). In our case, in which the environment transmits information to the user in one direction and touch involves a more complex activity compared to drag-and-drop or click on a touchscreen, a latency even in the order of seconds can be tolerated [29]. To enable environmental exploration, it is essential that received data is transmitted to a more complex portable device so that it can be processed to be converted into other kinds of feedback, e.g., auditory, haptic (vibration), or even, depending on the environment extension and on the application, logged on the Cloud. Therefore, to maximize connectivity, a wearable node needs to include a wireless transceiver normally present in consumer smartphone or tablets. Compared to [4], BT connectivity is increasingly preferred instead of Wi-Fi to reduce power consumption. In our context, BT can be effectively used thanks to the low data rate requirements of the application specified in [14]. At the same time, at a fixed node side the presence of wireless connectivity is still fundamental, but to enable landmark configurability or dynamic information transmission (landmark data can change over time).

B. Architecture

Fig. 2 shows a conceptual scheme of our *Live Wire* BCC. It comprises a TX that must be connected through a low-impedance path to ground. The TX drives a high impedance load, which is the human body, that in standard operating conditions is floating. A wearable RX, that is capacitively
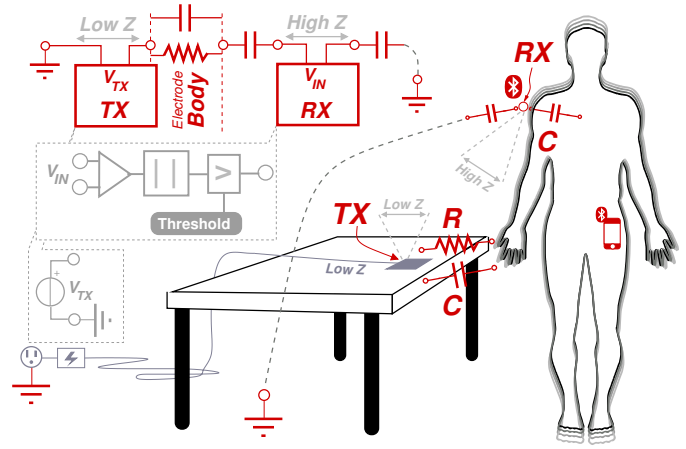

Fig. 2. Block scheme of the *Live Wire* BCC system.

coupled through the body and to the return path to ground, detects the signal through a high impedance input stage. The current required to operate the system, similarly to other capacitive BCC systems, is extremely limited by construction, accounting few tens of nA only. The TX can be implemented using a simple microcontroller that drives the TX electrode that overall is loaded capacitively.

The RX is in charge of amplifying, demodulating and synchronizing the incoming modulated signal, which has a sub-MHz center frequency. In our implementation a 550 kHz center frequency, corresponding to the highest speed achieved using our μPython rapid prototyping software solution, is used. This frequency falls in the interval used in commercial solutions and permit low-complexity transmission [26]. Thanks to its inherent non-coherent and non-linear nature, the RX is able to detect distorted signals, therefore enabling constraints to be relaxed for the TX as well. Indeed, a perfectly sinusoidal output is not strictly required, and modulation synthesis can be done by square waves, enabling the use of any digital General Purpose Input/Output (GPIO) in the TX microcontroller, that typically operates in a $3-5$ V range. The full swing signal drives directly the human body, to which the RX couples. It exploits a square electrode (in principle non in contact with the skin) and the PCB ground to create a capacitive coupling.

The tens of mV signal coupled at the RX input can be then amplified using a low-complexity front-end, rectified, thresholded and then sampled (at baseband speed, i.e., symbol rate) using, similarly, a GPIO generic input of a microcontroller. The processor can implement, in a software-defined fashion, both demodulation and synchronization. Unlike typical state-of-the-art solutions, in which RX are based on e.g., down-conversion [4], Orthogonal Frequency Domain Multiplexing (OFDM) [18], wideband signaling [30], super-regeneration [31] or injection locking [32], similarly to [7], the *Live Wire* RX rectifies the complete incoming wave, therefore including both signal and other potential disturbances that may be coupled through the human body. This assumption implies a lower complexity hardware compared to standard solutions, while not significantly impacting on performance, as will be further demonstrated in Sec. VI.
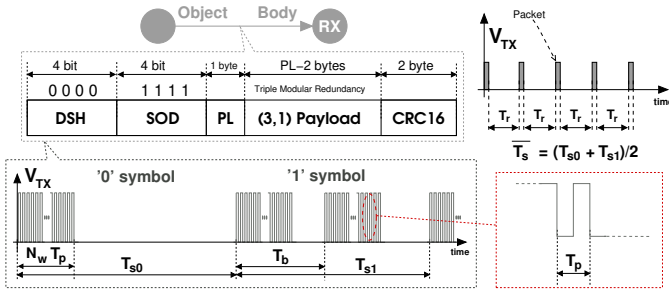
Fig. 3. S-OOK modulation, here asymmetric with different symbol duration for '0' and '1', with packet format and periodic TX access.
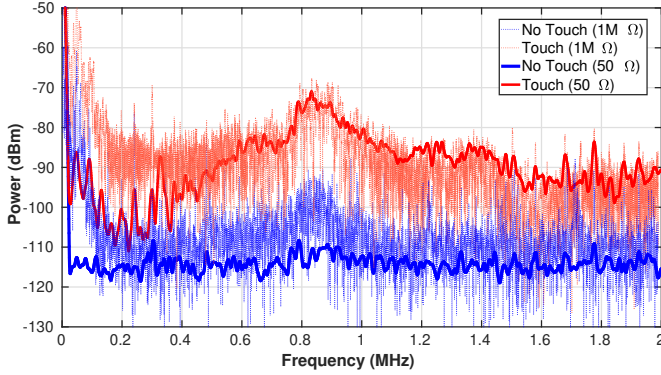

Fig. 4. Measured input power from the human body using a 3×2 cm electrode connected to a $50\,\Omega$ input RSA3408B real-time spectrum analyzer (resolution bandwidth 10 kHz), and to a DSO9404A (Fast Fourier Transform, resolution bandwidth 625 Hz, input impedance $1\,\mathrm{M}\Omega$). The background levels corresponding to a no touch condition, are depicted for both cases.

C. Modulation and Signaling

In terms of physical-layer modulation, BCC can encompass very different modulation techniques, ranging Quadrature-Phase Shift Keying (Q-PSK) [28], Bi-Phase Shift Keying (B-PSK) or On-Off Keying (OOK) [33]. In this work we have selected a self-synchronized version of OOK [an on/off digital variant of Amplitude Shift Keying (ASK)] thanks to its advantages in terms of power consumption (i.e., transmitter circuit active only when a '1' symbol is transmitted). OOK modulation is indeed a typical choice in capacitive BCC [4]. ASK, *inter alia*, is more suitable for short-range implant devices and telemetry systems with respect Frequency Shift Keying (FSK) and PSK, thanks to its simple associated hardware implementation and resulting size [34].

Fig. 3 shows the *Live Wire* Synchronized-On Off Keying (S-OOK) modulation format. The pulses center frequency is $1/T_\mathrm{p}$. Each symbol comprises a square wave of N_w periods (overall lasting $N_\mathrm{w}T_\mathrm{p}$), sync-to-sync pulse delays $T_{\mathrm{s}0}$ and $T_{\mathrm{s}1}$ (average symbol timing $\overline{T_\mathrm{s}}$) and sync-to-data delay T_b. T_r is the packet repetition delay. Observe that, in S-OOK, it is not required that symbol duration is equal for both a '0' and '1' symbol, while it is necessary that synch-to-data delay is controlled [35], even with low accuracy. At implementation-level this enables relaxation in terms of signal generation timing, thus tolerating mismatch between '0' and '1' symbol duration. This is beneficial especially when modulation and demodulation are implemented at software-level, hence relaxing constraints on

context switching delay between processes.

Packets comprise a Data Synchronization Header (DSH), a Start-Of-frame Delimiter (SOD), a Packet Length field (PL), a Payload and a Cyclic Redundancy Check (CRC). To ensure a reliable data transmission during landmark identification, indeed, the transmission needs to consider both a CRC for each packet and and Error Correction Code (ECC) so that symbols can be recovered also in case of bit flips due to noise and disturbance introduced by the body channel. *Live Wire* uses a CRC-16-CCITT standard CRC which has been extensively used e.g., for Bluetooth® and XMODEM. This CRC has been selected because packet length can vary, for our application from few to up to dozens of bytes. The selection of ECC codes used, at least in Wireless Sensor Networks (WSN), varies based on an implementation power consumption and performance trade-off [36]. *Live Wire* is based on a relatively high SNR transmission using very low power. Communication needs to be established only if the transmitter is in contact with the human body. Therefore, we have selected a very low complexity (3,1) Hamming code (triple modular redundancy) towards the energy efficiency side. All packet parameters are defined at software-level and can be modified according to the application. In this implementation both DSH and SOD have a fixed length of 4 bit. PL has a length of 1 byte and the payload length is variable between 0 and 255 byte. The CRC-16-CCITT length, computed on the (3,1) encoded payload, is 2 byte. In terms of channel access, the TX anchor, that receives an AC network-derived power supply and a ground reference through the USB port, continuously transmits packets using a periodical access with a delay of T_r between contiguous packets.

In *Live Wire* system latency can be specifically designed based on symbol timing, packets repetition frequency and length. In general, packet timing must satisfy the inequality $\overline{T_\mathrm{s}}8N_\mathrm{bytes} + T_\mathrm{r} < \Delta_L$, where Δ_L is the posed system latency and N_bytes is the number of bytes in the packet. Observe that if for a 2 bytes payload, including for instance one byte that codifies the landmark and another that carries status information, $T_\mathrm{r} = 50$ ms and $\overline{T_\mathrm{s}} = 909\,\mu$s, by considering coding we obtain $122\,\mathrm{ms} < \Delta_L$, which still satisfies the latency of human perception considered in literature.

D. Threshold Control

Fig. 4 shows the effect of touching a copper electrode (wire length 13 cm and connected to a female SMA connector) referred to the AC power distribution ground, using a $50\,\Omega$ input spectrum analyzer and a $1\,\mathrm{M}\Omega$ input impedance oscilloscope in a laboratory environment. When the TX electrode is in contact with the human body, therefore it is shunted to a low-impedance path to ground, the body captures interference sources in the environment and operates as a wire (or an antenna below 200 MHz thanks to its high dielectric constant [37]). In a 500 kHz bandwidth (center frequency 500 kHz), on a $1\,\mathrm{M}\Omega$ impedance, an overall average power of -44 dBm is available at the receiver input, that corresponds to an average input voltage V_RX of $\sim$180 mV (computed from $P_\mathrm{IN} = \frac{V_\mathrm{RX}^2}{R}$, where P_IN is power and $R = 1\mathrm{M}\Omega$). In case of no touch, the
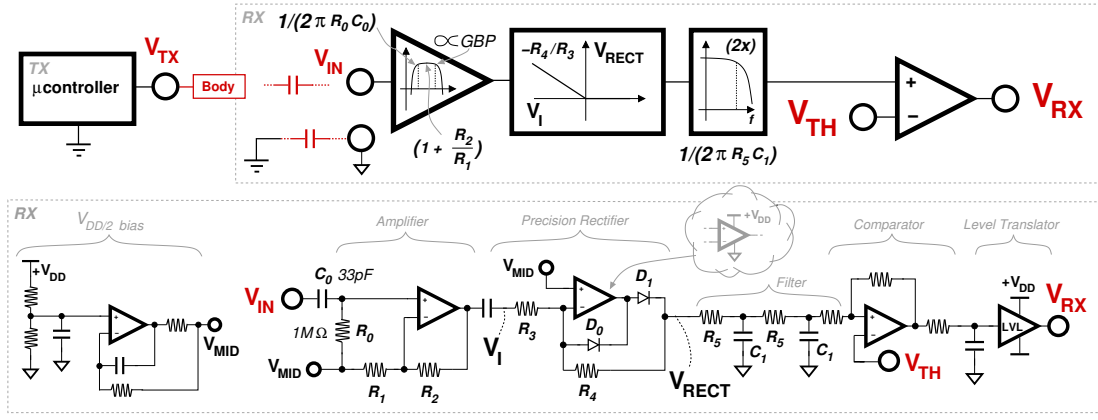
Fig. 5. *Live Wire* block scheme and RX front-end schematic.

average input power is on the order of -68 dBm, which is translated into a V_{RX} of $\sim$13 mV.

These average figures of merit are an indication of the disturbance power level that may be captured by the receiver, and confirm that interference is captured by our high input impedance front-end and most important, disturbance is dynamical and highly depending on the surrounding environment including existing wireless networks [37]. For this reasons, the *Live Wire* RX shall be able to adjust the threshold used to demodulate data. Threshold control does not represent for our system a significant complexity point: it can be achieved, as will be detailed next, using a simple algorithm that starts from a minimum threshold level and increases it linearly until no noise or interference triggers are present. With an energy detection front-end, such linear threshold adjustment is an effective solution in cognitive radios [38]. These radios, dynamically configure front-end to achieve the best performance in presence of interference and prevent congestion. In our context the problem to be solved is similar, because the receiver does not need to be jammed in presence of large interference.

IV. HARDWARE DESIGN

A. Block Scheme and RX Front-end

Fig. 5 shows a block scheme of our *Live Wire* prototype, with a detail on the schematic of the RX front-end. As previously introduced, the transmitter is based on a low-impedance GPIO output of a $\sim$3 V powered microcontroller, that can be software programmed. The RX front-end comprises an amplifier, a rectifier a low-pass filter and a continuous time threshold comparator. The incoming BCC signaling wave is amplified using a high gain-bandwidth product single rail AD8028A OpAmp, to enable the reception of pulses with center frequency in the range 5 kHz$-$1 MHz, thus providing a larger degree of freedom for the development. Moreover, to minimize the number of energy sources, the amplification front-end has a single power supply. Non-coherent detection is provided by the Precision Rectifier, whose output is filtered and thresholded using the comparator that has a positive feedback to introduce hysteresis, implemented with the same OpAmp. The reference voltage V_{MID} is derived

from the 2.83 V voltage supply V_{DD}, divided by two by a voltage divider (left) and buffered using an OpAmp. The first Amplifier stage does not include capacitors to fully exploit the high Gain-Bandwidth Product (GBP) of the OpAmp, and has a nominal gain of 30 dB.

The system implements AC mains supply (50 Hz nominal frequency in Europe) noise filtering using the high pass filter made of C_0 and R_0, nominally 33 pF and 1 MΩ, which corresponds to a -3 dB cut-off frequency of 4.8 kHz. As the AD8028A provides a dedicated stand-by signal, the front-end can be now turned off by the microcontroller in idle state to save power (signal not shown for the sake of brevity). The rectifier, that provides phase inversion for negative signal values, has a nominal gain of 47. The Shottky diodes D_0 and D_1 in the rectifier are CFSH-4. After rectification the signal is low-pass filtered using a two poles low-pass filter implemented with R_5 and C_1, providing a cut-off frequency of 125 kHz. Nominally, R_0=1 MΩ, R_1=10 kΩ, R_2=330 kΩ, C_0=33 pF, C_1=47 pF, R_3=4.7 kΩ, R_4=220 kΩ and R_5=27 kΩ.

B. TX and RX PCB Modules

Fig. 6 shows the block scheme of both wearable and anchor nodes, i.e., RX and TX, respectively. As transmission is based on high-impedance signaling, TX symbols generation is simply implemented using a GPIO output of a microcontroller running digital $0-V_{DD}$ transitions. This pin, is directly connected though a decoupling capacitor to a metallic pick-up, that, in turn, can be fixed to an anchor object. By touching the metallic element, as previously discussed, the human body turns into a "wire", allowing the RX to capture TX symbols thanks to an high input impedance of $\sim$1 MΩ. Both TX and RX devices comprise an L-series STM32L486 MPU, running μPy version 1.9.1, that we have ported (and patched to enable the use on-chip DAC) from the officially supported F-series STM32 port [19]. The modules comprise the Bluegiga BGM123A module that communicates with the μcontroller that transmits commands and receives BT events through a Universal Asynchronous Receive and Transmit UART port configured with enabled flow control. Both devices provide μUSB connectors to enable power supply/battery recharge using a BQ24230 and TPS78001, LDO and battery charger, respec-

Fig. 6. μPython-based RX (wearable node) and TX (anchor node) block scheme comprising wireless interconnection with an external smartphone.

tively (3.7 V, 250 mAh nominal capacity). The power supply is set to 2.83 V, the minimum voltage to enable all components operation, maintaining a lower power consumption compared to the standard 3.3 V supply. This way, as battery voltage decreases, the available charge can be exploited as much as possible and increase device lifetime. For the TX (which, in any case, needs to be connected to the infrastructure) the LiPo battery operates as a back-up in case the voltage supply provided by the μUSB connector is interrupted. The TX series decoupling capacitor has a nominal value of 4.7 nF. Observe that such capacitor has an impedance at 550 kHz as low as $\sim$62 Ω, therefore not significantly impacting on the conceptual transmission scheme previously described.

The analog front-end, has a threshold V_{TH} controlled by a first STM32 DAC (`DAC1` in figure). The asynchronous events (`Asynch. Evt.`) received from the RX front-end are transferred to a general purpose digital I/O of the μcontroller. The RX module comprises both a DRV2605 vibromotor driver connected to the microprocessor through an `I2C` interface, and a TS421IST mono headphone amplifier (with the corresponding 3.5 in connector) directly driven by a second STM32 DAC [`DAC2` in Fig. 6]. Both TX and RX systems can be programmed through a dedicated connector and a full-custom programming board (not shown) using a `JTAG` and a `SWD` interface, for the MPU and the BT 4.2 chip, respectively. The RX μcontroller is connected through a Quad-SPI port (`4bit MMC` interface) using an SMD connector to an external SD-card, that is powered using the 2.83 V main voltage supply. Finally, the RX board comprises a buzzer connected to the MPU using a dedicated `GPIO`.

The BT 4.2 link, at the RX side, enables push notifications to a portable device. At the TX side, BT can be used to update configuration or update anchor status data with wearable nodes information. The TX BT transceiver can be also utilized jointly with the BCC link to implement a full duplex communication with the anchor node. A portable device, such as a smartphone, upon reception of an event from the anchor through the BCC PHY link, can then establish a BT connection with the TX and exchange information.

V. FIRMWARE DESIGN

A. TX

The BCC signaling waveform is digitally generated by a TX `GPIO` using the μPy Viper code emitter [39]. In our implementation, T_r can vary. For our error-rate tests we kept $T_r = 250$ ms for ease of testability, while for other functional tests we kept $T_r = 50$ ms. T_{s0} is 848 μs, T_{s1} is 970 μs, T_b is 520 μs, pulses center frequency is 550 kHz and N_w=96. The pulse parameters have been selected based on extensive functional tests in the environments of Fig. 17(a).

B. RX Synchronization and Demodulation

Fig. 7 shows a simplified flow chart of the RX firmware. The signal detection loop inherently includes a Clear Channel Assessment (CCA) based on a rectifier (similar to an energy detector [40]), which is used to establish the absence of a transmitted signal, and in turn run threshold control and adjust the front-end selectivity to minimize error-rate and avoid RX jamming. The *Live Wire* TX electrode (or the associated object), that repeatedly transmits packets, can be touched anytime and in general asynchronously by the user, also during the transmittal of a packet, which opens the way of a series of cases that the receiver needs to handle to ensure service availability. During the main loop start-up (left), after peripherals initialization (including GPIO, front-end, headphone driver, vibromotor) and internal variables reset, the system updates the BT chip status, to make sure the radio is set in advertising mode, hence discoverable by other devices. Demodulation and synchronization is based on a continuous polling on V_{RX} based on an iteration counter `num`, a symbol number counter `lp`, a timeout counter `num_to`, a last symbol detection counter `timenow` and a set of status flags to identify the various PHY packet fields. The idea is to continuously check for a GPIO transition, and if detected, decode a symbol (and check the corresponding delayed data bit through another GPIO read, not shown in the flow chart) and update a vector of received symbols `RX_SYM_VECT` that in turn needs to be tracked at every iteration. The internal logic routine `Decode packet (lp)` keeps track of the progressive reception of the symbols and returns continuation, valid and invalid conditions depending on the content of `RX_SYM_VECT`. If a packet is correctly received (the CRC is correct), the received payload is sent to the BT (`Write BT Characteristic`) that, if connected, transmits the data (notification) to the connected device. After transmission the system plays a wave file or alternatively buzzes a sound and restarts from threshold adjustment. In case of an invalid packet (incorrect CRC or DSH/SOD) the status variables are simply reset to restart from `Adjust THR`, the routine that controls threshold that will be detailed next. This corresponds to the condition `THR Error`, i.e., threshold control is re-initiated because the packet reception sequence has been interrupted.
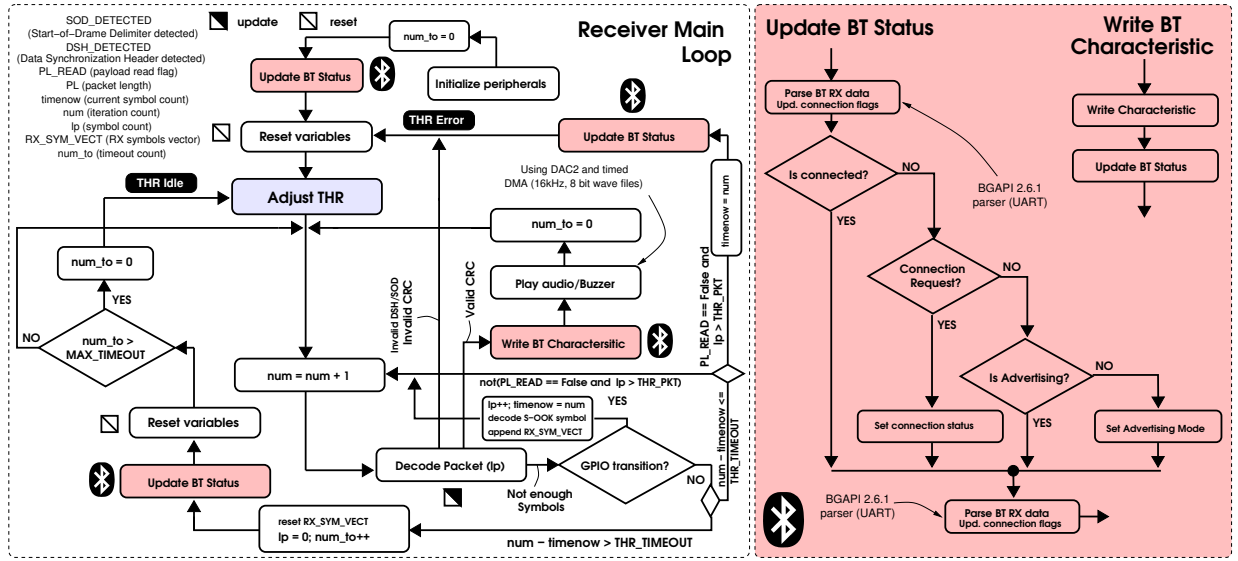
Fig. 7. **(left)** RX main infinite loop controlling both PHY layer, BT communication and module I/O peripherals, **(right)** detail on the BT status update routine.

Algorithm 1: Threshold Control

Result: DAC output V_{TH} for the RX front-end.

$THR = THR_{min}$;
$V_{TH} = V_{DD} THR / 255$;
$\tau = 0$;
$t = 0$;
while $\tau \leq T_{timeout}$ **do**
    while $t \leq T_{min}$ **do**
        $\tau = 0$;
        if $V_{RX} = {}'1'$ **then**
            $t = 0$;
            $THR = THR + 1$;
            $V_{TH} = V_{DD} THR / 255$;
            Wait for Δt_{on};
        else
            $t = t + \Delta t$;
        end
        Wait for Δt;
    end
    if $V_{RX} = {}'1'$ **then**
        $t = 0$;
        $THR = THR + 1$;
        $V_{TH} = V_{DD} THR / 255$;
        Wait for Δt_{on};
    else
        $\tau = \tau + \Delta t$;
    end
    Wait for Δt;
end
Update V_{THR} with THR (fixed length M);
$THR = \overline{V_{THR}}$;
$V_{TH} = V_{DD} THR / 255$;

To ensure a correct reception this simple mechanism is not enough as it may happen that due to insufficient signal drive symbols are not received correctly. To overcome this problem two restart conditions are given using two thresholds, a symbol duration timeout (THR_TIMEOUT) and a packet length threshold (THR_PKT). The first threshold is used to detect a timeout after a symbol is received: as the transmitted symbols have a fixed $T_{s0} + T_b$, waiting more than the expected symbol duration is an indication of reception of an end of a corrupted packet. The system can then increase the timeout counter num_to and reset the received symbol counter lp with the corresponding vector, variables and restart without threshold adjustment because the touch event started during the transmission of a packet, therefore RX shall immediately capture the next transmitted packet. If packet reception is not completed successfully after a number of trials MAX_TIMEOUT, the system restarts from threshold adjustment, even if the subject is still touching the TX electrode. Observe that linear threshold adjustment, notwithstanding being an heuristic approach, can operate also in presence of a busy channel [38]. In the diagram, this new threshold adjustment corresponds to the condition THR Idle. The use of the second threshold THR_PKT is combined with a condition on the ongoing payload demodulation, that is (PL_READ == False and lp > THR_PKT), where PL_READ is a flag that indicates that payload is being read. If the system status after THR_PKT symbols is not reading the payload, the loop is restarted (with variables reset) again from threshold adjustment to indicate that a touch event occurred within a packet transmission.

C. RX Threshold Control

Alg. 1 shows a conceptual representation of the threshold control algorithm. Similarly to an ED-based CCA, our threshold adjustment is low-complexity, and it does not need to be run continuously. Consequently, it can be activated on demand and run for a limited amount of time to minimize

power consumption. The ED-based threshold control algorithm is based on a linear threshold increase starting from a minimum value $\text{THR} = \text{THR}_{min}$ until V_{RX} is always sampled '0' within a T_{min} interval. Within T_{min}, if V_{RX} is '1', threshold is increased by 1, i.e., $\text{THR} = \text{THR} + 1$, and the DAC is set to THR. Once threshold is set and stable so that this condition occurs, the algorithm checks if V_{RX} is '0' within an additional duration $T_{timeout}$. If V_{RX} is sampled '1' within $T_{timeout}$, threshold is increased, timeout counter is reinitialized and a check within T_{min} is reinforced. If V_{RX} is sampled '0' within $T_{timeout}$ the algorithm appends the current threshold to a vector of M elements V_{THR}, computes the average threshold $\text{THR} = \overline{V_{THR}}$, sets the DAC to $\overline{V_{THR}}$ and exits. In the algorithm we schematized the two counters for THR_{min} and $T_{timeout}$ using two independent variables t and τ. To take into account for a setup time or the front-end comparator the algorithm waits for a duration Δt. When the condition $V_{RX} = '1'$ is triggered the system waits for an additional Δt_{on} hold-off time for the comparator. Voltage V_{TH} is computed based on the microprocessor supply voltage V_{DD} and on the used resolution of the DAC, in our case, 8 bit. Observe that provided that threshold is set high enough, it exists a condition so that V_{RX} is always '0', therefore ensuring that the loop always exits. This condition has been extensively demonstrated through the measurements presented in Sec. VI. This simple algorithm is quite effective even when run during a partial packet reception.

Fig. 8. **(top)** *Live Wire* prototype (TX and RX) and corresponding iOS phone running an application that receives push notification through BT, and **(bottom)** photograph of TX and RX PCB with physical size.

D. Bluetooth® Management

A subset of the commands and events specified in the Bluetooth® BGAPI version 2.6.1 reference manual [41] have been ported in a specific μPython library implementing packet encapsulation, parsing and decoding of the received event data. The BGAPI library specify the format of the data,

control and event packets that need to be transmitted and received to the BT chip through the PHY interface, in our case a dedicated UART. In this implementation the device can handle a single connection. This is reasonable as the present system is intended to be a personal device, therefore a single client, e.g., a smartphone, needs to be connected at a time. `Update BT Status` (on the right) parses first any packet from the BT UART port (including events received from the radio front-end) and based on the received packets updates connection status flags. If not connected, the device checks if a connection request has been made and if not, sets the device in advertising mode. Lastly, the BT UART output is parsed again to check if advertising mode has been correctly set by the chip. Observe that the BT chip is fully autonomous w.r.t. the STM32 microprocessor, hence once in advertising mode, the BT chip asynchronously generates UART packets to inform the STM32 of stage changes.

VI. MEASUREMENTS

A. Prototype and Proof-of-Concept iOS Application

We have implemented the TX and RX modules shown in Fig. 8, using a standard FR4 dielectric. The RX comprises a copper electrode of size $5.5\,\text{cm} \times 3.6\,\text{cm}$. The TX electrode has a size of $4\,\text{cm} \times 3\,\text{cm}$. To demonstrate the possibility of transmitting push notifications to a more complex and multisensory device that handles elaborated audio and haptic feedback we have implemented a full-custom smartphone application on an Apple® iPhone 8 smartphone running iOS 12. The *Live Wire* agent application once loaded runs in background and provides a text-to-speech output of the content of the payload received through the BCC. The very first time the application is launched a default BCC device needs to be specified (through the CCID automatically generated by the operating system). After this step, the smartphone automatically connects to the specified *Live Wire* RX every time the application is loaded, providing sound alerts in case the RX is out-of-range or the Bluetooth® central manager is turned off. The data transmission from the BCC device to the smartphone is based on a BT notifications mechanism.

B. Test setup

To verify the correct operation of *Live Wire* and to establish its performance figures, we have designed a specific setup. During the tests, we keep the reference electrode (i.e., the PCB ground plane) of the RX module floating, as in an ordinary operating condition. Grounding the RX would cause a coupling between V_{IN} and the interference sources of the power supply terminals, therefore impacting on packet error rate. We implemented a μPy BT streaming routine that transmits both the ADC-sampled output of the front-end, and the main algorithm threshold adjustment phases. At the TX side, we can run both transmission of random packets to establish packet-error rate, or a simple square wave at 550 kHz to establish SNR at the RX input, and consequent signal level at its input. Fig. 9(a) shows the measurement setup, consisting of a TX plus electrode located on a desk, connected to a PC which provides a BT connection through a dedicated USB Bluegiga
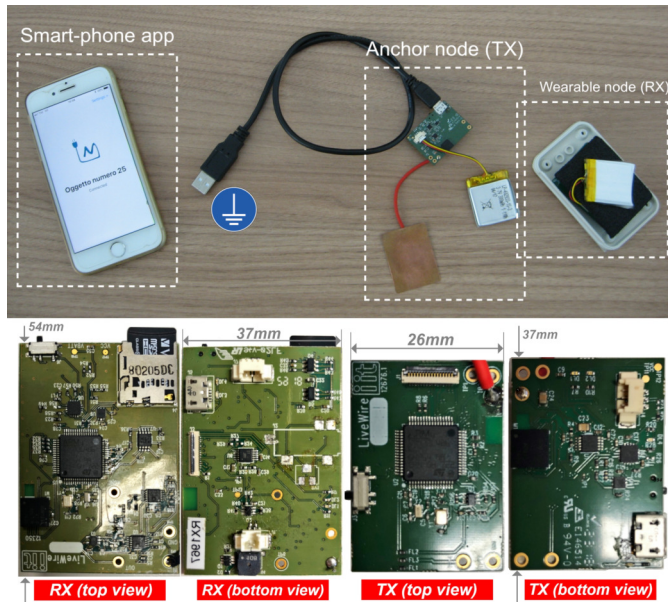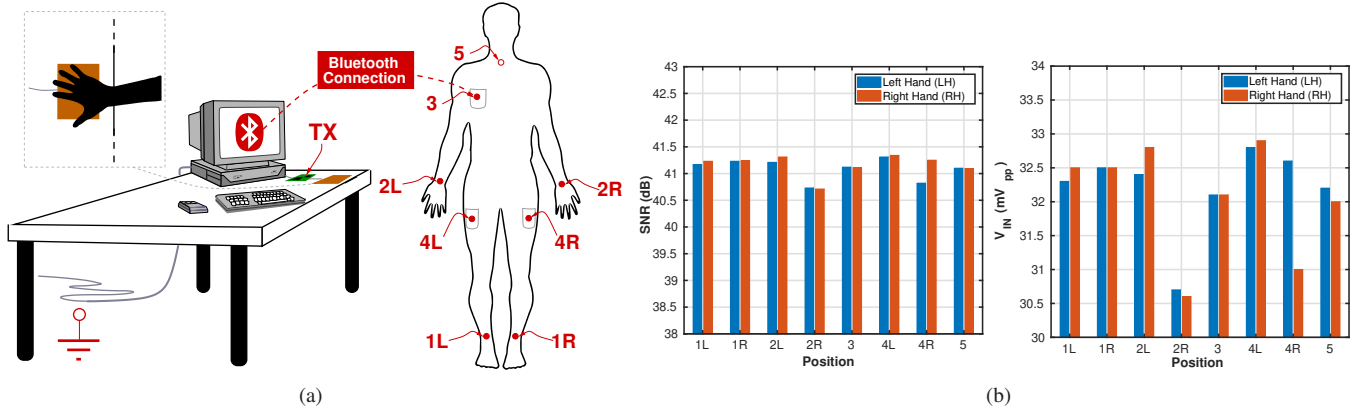
Fig. 9. **(a)** SNR setup of the input signal when the TX is touched using the left or the right hand (LH, RH) with the RX in different body positions. **(b)** Measured SNR and input-referred signal level (front-end $G = 22$), 10 MHz input referred noise bandwidth.
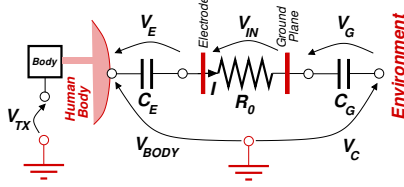

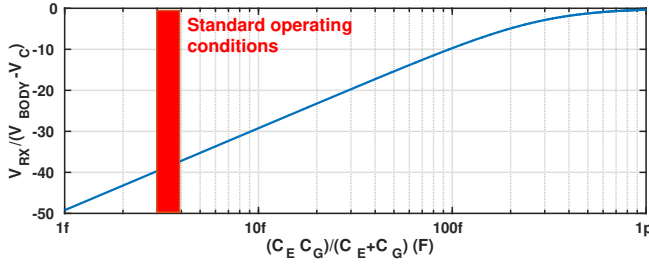Fig. 10. Simplified lumped model to quantify coupling order of magnitude (quasi-static near-field).

Fig. 11. Signal loss as a function of the series of ground plane and electrode coupling capacitance $\frac{C_E C_G}{C_E + C_G}$.

TABLE I
MULTIPLE SUBJECTS SOFT BIOMETRIC DATA

Subject Number	Gender	Age (years)	Height (m)	Weight (kg)
1	Male	25	1.87	82
2	Female	24	1.65	60
3	Male	25	1.83	65
4	Female	18	1.62	57
5	Female	25	1.60	60
6	Female	24	1.62	58
7	Male	24	1.75	68
8	Female	24	1.60	62
9	Male	25	1.80	70
10	Male	25	1.70	71

BT 4.0 dongle. We ran measurements on a single subject and we confirmed SNR findings over subsequent multiple subjects. For the former, the RX is worn by a male subject, 174 m height, 78 Kg weight, aged 37, in different positions (the RX is fixed using an elastic band and the electrode, facing the skin, is not in contact with the skin but with the garment) according to the sketch [for position 3 in Fig. 9(b), the RX is worn in subject's shirt pocket]. For the latter multiple subject measurements, overall ten people was involved. Their soft biometric data shown in Tab. I. Data is acquired using a Python utility program running on the PC, and then elaborated using Matlab®.

C. Live Wire Signal Level

Fig. 9(b) shows the measured SNR and signal level V_{IN} obtained using the TX in Continuous Wave (CW) mode (550 kHz square wave), in different locations on the body, namely 1L, 1R, 2L, 3, 2R, 4L, 4R, and 5, by touching the TX electrode using both the left and the right hand (LH, RH, respectively). Based on a measured gain front-end G of 22 (lower compared to the design due to losses of the PCB components), we have extracted both SNR and equivalent input voltage V_{IN}. The result is that the SNR is constant throughout the body with a ~0.5 dB variation. This effect is given by the low-impedance node to ground provided by construction at the TX.

To understand the order of magnitude of the quantities involved in the transmission, we report the lumped model schematized in Fig. 10. Once the transmitter is touched the ~3 V signal that is generated across the electrode terminal is transferred to the human body that emits the signal. We assume that skin-to-electrode contact impedance is in the same order of magnitude of the input impedance of the RX input stage (very high and 1 MΩ in this implementation). In general, BCC signal propagation can be explained using the several works available in literature to model the human body (in general a network of parallel capacitive and resistive impedance). However, at such low frequency, i.e., 100 kHz−40 MHz, the human body electric field can be considered as quasi-static near-field [4]. Based on our experimental data, at 550 kHz center frequency through the TX, can be received with a 0.83 dB signal loss using an electrode in contact with the skin, referred to the same ground of the TX. This number is obtained using an oscilloscope probe at 10 MΩ impedance, therefore detecting voltages of ~3 V (i.e., the measured voltage, referred to ground on the human body), resulting in peak currents of 300 nA, for a total power dissipation of 30 nW on the human
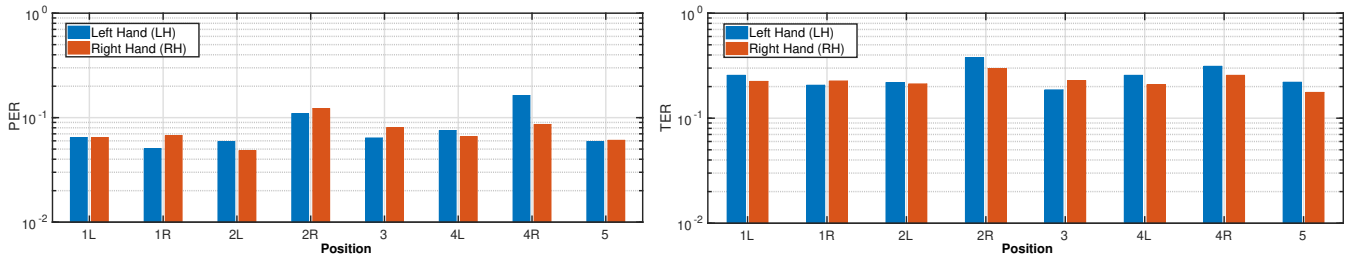
Fig. 12. Packet and Total Error Rate as a function of the positions of the RX on the human body given in Fig. 9(a).

body in this condition. This value is well below the safety limits stated in [42], that are considered by state-of-the-art works [4].

We can collapse the core transmission parameters in two equivalent capacitive contributions between the two electrodes. In turn the RX that is worn on the body can capture the radiated signal, thanks to the coupling between the electrode terminal to the body and the environment (ground). The coupling, in absence of contact with the electrode is capacitive, and the current flow depends on the series of these two capacitance contributions C_E and C_G, the to-body and to-ground coupling capacitance, respectively. The RX has a very high input impedance that can be modeled as R_0. The current that flows through the body and ground can be determined using the Kirchhoff Voltage and Current law, across and through the nodes specified in the schematic of Fig. 10.

By neglecting the intermediate calculations, the voltage across the input stage of the RX can be expressed as,

$$V_{IN} = (V_{BODY} - V_C) \frac{s R_0 C_G C_E}{C_G + C_E} \Big/ \left(1 + s \frac{R_0 C_G C_E}{C_G + C_E}\right), \tag{1}$$

where V_{BODY} is the ground referred voltage across the human body, V_C, normally zero, is used to model shunt effect. Observe that the RX system is non-coherent, therefore the RX electrode positioning can be flipped, i.e., the PCB ground plane can face the body while the electrode can face the environment. In presence of standard operating conditions $V_C \sim 0$, while in presence of the shunt effects, experimentally determined in Sec. VI-F (that is both PCB plane and electrode are both coupled to the body, only), $V_{BODY} - V_C \sim 0$, i.e., $V_{BODY} \sim V_C$.

Fig. 11 shows a plot of Eqn. (1) as a function of the series capacitance $\frac{C_E C_G}{C_E + C_G}$. Using the test setup depicted in Fig. 9(a)(left), as the input voltage across the RX input stage is about ~ 33 mV, we can extract an approximate value of the series capacitance that leads to correct device operation, in absence of body shunt, which is between 3 fF and 4 fF. Observe that the smallest contribution is given by the C_G which needs to be undoubtedly lower compared to C_E, as the body-to-RX separation is times lower compared to PCB-plane to ground separation. The current that flows in the RX during a pulse transmission is then ~ 33 nA. Observe that the given coupling capacitance range is consistent with the measurements depicted in [15], in which the backwards capacitance falls to ~ 100 fF for backwards path lengths of 30 cm. In this case, the backwards return path is substantially more, therefore leading to a very low coupling. The obtained loss, i.e., ~ 19.3 dB is comparable to the Single-Ended TX−Single-Ended RX case shown in [8], with the difference that the TX in our case has a low-impedance path to ground. In [8], path loss is about ~ 8 dB higher [see Fig. 7(c)], due to the TX coupling to ground through a capacitor rather than an equivalent resistor. Observe that in case an RX electrode is in contact with the skin, one between C_E or C_G would tend to ∞, therefore relying on the other capacitor coupling to ground.

D. Packet Error Rate

Fig. 12 shows the measured Packet Error Rate (PER) and Total Error Rate (TER) as a function of the positioning of the RX. Errors occur because channel injects noise and interference at the receiver input. The number of packet transmitted per test is $N_{TX} = 500$. The transmitted packets comprises two random digits (0–9), and three digits comprising a zero-padded progressive packet number, ASCII encoded (one byte per digit). The transmitter sends a new packet every 250 ms. We define PER, as N_{CRC}/N_{RX}, and TER, as N_{RX}/N_{TX}, where N_{CRC} are packets with CRC errors, N_{RX} is the number of packets correctly received out of N_{TX}. Compared to PER, TER includes also a measure of missed packet synchronization. In this test, the RX is worn in the different body positions previously specified, the person stands and touches the TX in using both Left or Right Hand (LH and RH, respectively) for the complete transmission of the packets. Every time the RX detects a packet, it transmits the payload through the BT to the PC that associates a time-stamp. This way, we can post-process the received data and obtain all the error-rate figures of merit.

PER and TER are almost independent from the RX positioning on the human body leading to an average of ~ 0.1, ~ 0.25, respectively. The minimum achievable PER depends on software implementation. In our μPython solution we have kept the garbage collector enabled. Every 1/4 second, μPy starts its garbage collection process that has the highest priority among any other scheduled task, therefore leading to potential synchronization errors. By deactivating the garbage collector (even at firmware build time) performance can increase, therefore enabling even lower error-rates.

E. Threshold Control

Fig. 13(a) shows a transient plot of the threshold control loop operating when the RX is worn in position 3, without touching the TX (null input signal). In rest state the algorithm
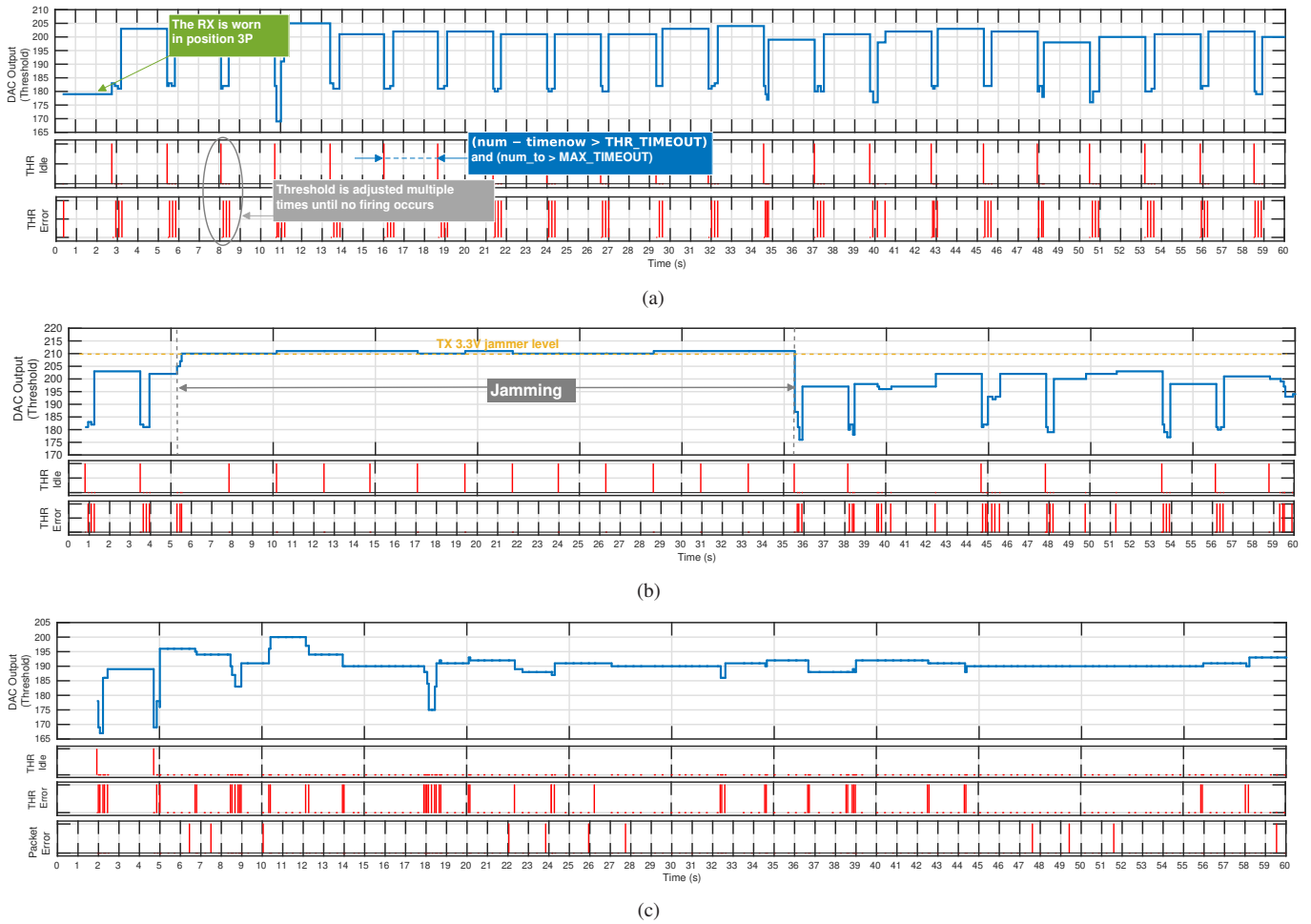
Fig. 13. Threshold adjustment cycles, **(a)** for configuration 3 given in Fig. 9(a) and 60 s operation without TX packets reception (no input), **(b)** with multiple jamming, i.e., when the subject repeatedly touches an electrode that generates a fixed 3.3 V square wave at 550 kHz frequency, **(c)** during a packet error ratio test, in position 5 (LH), with detail on threshold set events and packet error occurrences. Each depicted value represents the final output of `Adjust THR`.

cycles between `THR Errors` and `THR Timeout` event adjustments, continuously setting an average threshold of ∼190, that corresponds to 2.1 V. This simple test demonstrates that the algorithm converges as the initial threshold set condition is always fixed, and in presence of noise there is always an "escape" condition that leads `Adjust THR` to timeout.

Fig. 13(b) shows a transient plot of the threshold control loop when the subject multiply touches a copper electrode on which a 550 kHz square wave signal at 3.3 V is driven ("Jamming" indication). Once the receiver is jammed, the control loop maintains a high threshold output because the output of the front-end saturates. The `THR Idle` condition is continuously checked every time the timeout counter is triggered. As soon as the jamming ends, the system restores the previous threshold levels, through another threshold adjustment (lasting a timeout interval). This simple measurement results demonstrate that the control loop returns even in presence of continuous wave interference.

Threshold adjustment is demonstrated to be effective also in presence of a continuous packet transmission from the TX. Fig. 13(c) shows the evolution of the threshold set during a packet error-rate test in position 5. In these conditions, the algorithm successfully tracks the correct DAC level to maintain a steady threshold of ∼190, disregarding packet errors.

To better collocate the threshold set obtained during the error-rate test, by post-processing the received data through the BT link, we have extracted the distribution of the threshold sets over the multiple times the RX runs `Adjust THR`. Fig. 14 shows a histogram (ten bins each) of the threshold set for the correctly received packets only. From the results, it is straightforward that the threshold set strongly depends on the positioning of the device on the human body that captures external interference (that in any case varies over time).

To validate threshold control in presence of interference, we have connected an Agilent 33522A signal generator to the TX electrode and generated a continuous square wave. In this condition a packet error rate test is run. We observed that the result of the test strongly depends on the posture of the subject as well as its relative positioning with respect to the TX (see next subsection for further experiments and details). For instance, when the subject is standing tall, in position 3 [see Fig. 9(a)], a PER of 0.15 (TER of 0.352, average threshold 194) is obtained while injecting a $1\,V_{pp}$ signal on the TX electrode at 500 kHz center frequency. To enhance the interference impact we have repeated the tests when the
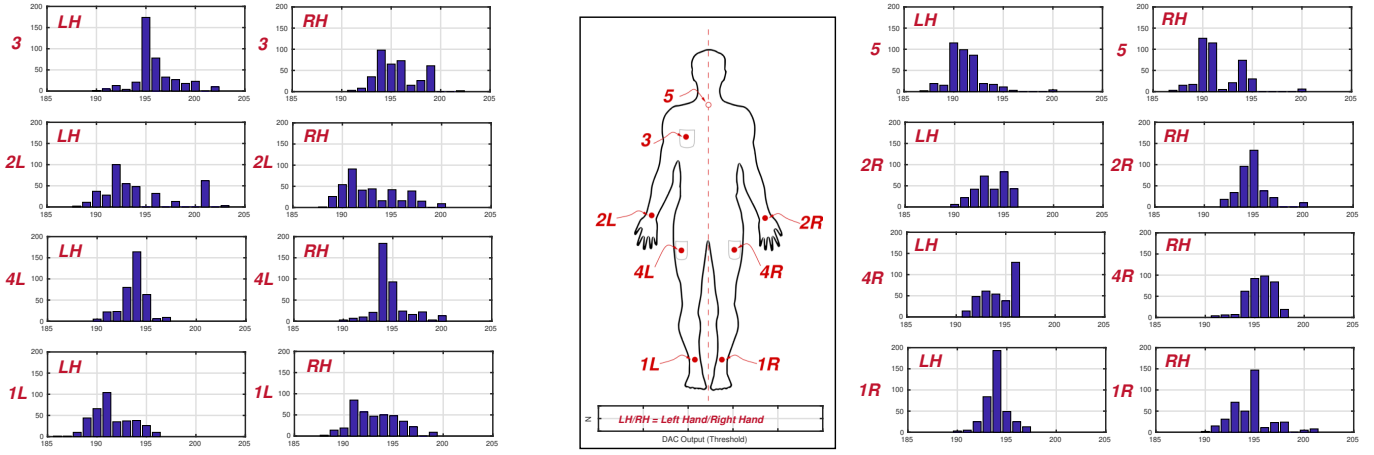
Fig. 14. Histogram of the threshold set corresponding to a correct packet reception as a function of the RX positioning, left and right hand touch (LH, RH). Axes units are specified below the body silhouette.
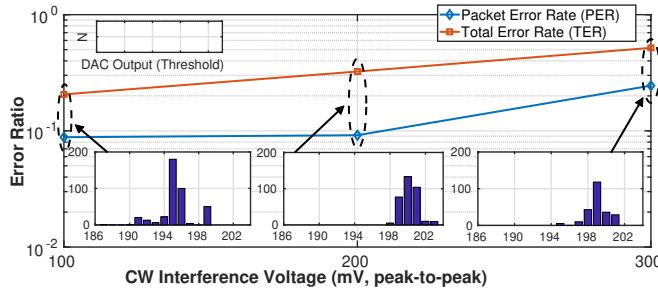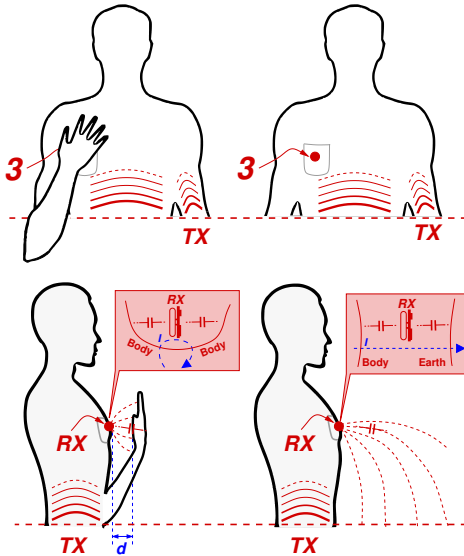

Fig. 15. Impact of CW interference on the performance of the system for different amplitudes, with threshold sets during the experiment corresponding to a correct reception.

Fig. 16. **(top)** Conceptual body shunt sketch. The human body, that is driven by the TX terminal "obscures" the RX, by shunting its terminals, and **(bottom)** measured SNR as a function of hand-to-device separation d.

d (cm)	SNR (dB)	V_{IN} (mV$_{pp}$)
0 – Complete Cover	6.74	0.6
2	26.54	6.0
5	38.27	23.1
10	39.13	25.5

subject is sitting on an anti-static chair in front of the desktop shown in Fig. 9(a), using exactly the same signal frequency of 550 kHz, same position 3, and touching the TX using the left hand. Fig. 15 shows the PER and TER degradation as a function of interference amplitude. At 300 mV amplitude the error-rates increase by a factor two. Observe that the threshold set for the three cases progressively increases as the CW interference contributes as an offset across V_{RX}. These tests demonstrate that the threshold control algorithm successfully counterbalances external disturbances even in presence of strong in-band interference.

To quantify the Signal-to-Interference Ratio (SIR) corresponding to each injected amplitude level we can compute the average power on the 1 MΩ load RX input, starting from the diagram of Fig. 3. By assuming packetizing, i.e., a transmitted number of bits N_{bit} (uniformly distributed), for an average duration of $\overline{T_s} = \frac{T_{s0}+T_{s1}}{2}$, and packet repetition T_r, SIR, defined as P_{TX}/P_I can be written as,

$$SIR = \frac{N_{bit}\overline{T_s}}{N_{bit}\overline{T_s} + T_r} \frac{V_{DD}^2}{2V_I^2} \left(N_w T_p/T_{s0} + 2N_w T_p/T_{s1} \right). \quad (2)$$

During our test, $N_{bit} = 48$ (including triple modular redundancy), $\overline{T_s} = 909\,\mu s$, $T_p = \frac{1}{550kHz}$, $V_{DD} = 2.83$ V. By using Eqn. (2), SIR is -3.9 dB for 1 V interference amplitude, and 40.7, 10.2 and 4.5 dB for 100, 200 and 300 mV_{pp}, respectively.

F. Body Shunt

Assuming same distance w.r.t. the skin, the to-ground RX coupling can significantly vary based on the body masking of the return path. Fig. 16(top) exemplifies the concept, we identify as "body shunt". When the RX is positioned in the subject pocket, the to-ground capacitance can be decreased by shielding the PCB ground plane using a hand. The received signal level is then a function of the spacing between the hand and the RX. Fig. 16(bottom) shows SNR measurement results as a function of the distance of the experimenter right hand w.r.t. the *Live Wire* RX. The shunt effect is not relevant for distance d greater than 10 cm, while it significantly degrades SNR as the hand gets closer to the device. Based on extensive
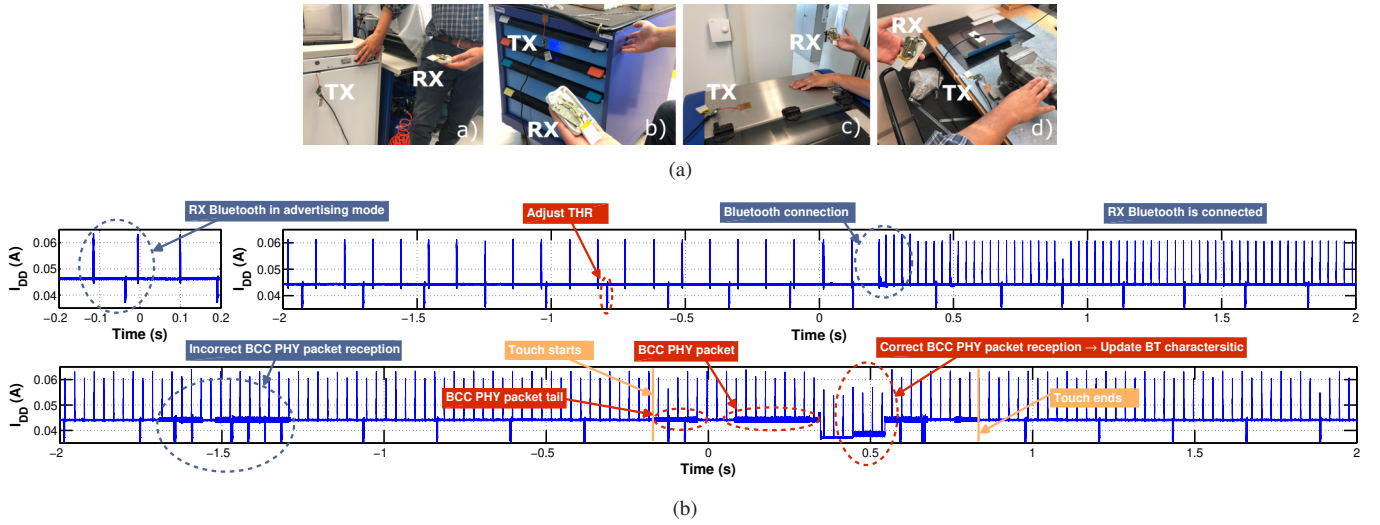
Fig. 17. **(a)** Different test conditions of the BCC system, with the TX connected through available USB ports in a laboratory environment. In all these conditions, the packets depicted in Fig. 3, are correctly received (no CRC error) from the RX device in the hand of the corresponding author. **(b)** Example measured RX current through the battery terminals during operation (no buzzer and no audio wave play).

experiments, we have understood that this shunt phenomena can severely decrease signal level, while people garment (e.g., shirts, jackets, sweaters) does not impact significantly on signal level degradation. We conclude that the positioning of the RX device shall account for this degradation and it needs to be worn so that this effect is minimized during its normal use. Alternatively, the front-end gain can be significantly increased to detect lower input voltages V_{IN} without compromising the required touch-only responsiveness, in any case.

G. Functional Tests

Fig. 17(a) shows a collection of four test conditions in a laboratory environment for a successful transmission. The TX is installed using the available USB port of nearby PC, and the correct operation of the RX is confirmed by an acoustic signal every time a correct payload is received. In turn the RX is connected through BT (in 4.2 mode, hence, with a payload larger than 20 byte) to the smartphone that provides push text-to-speech notifications once an object is touched. The TX firmware runs a continuous packet transmission containing an ASCII payload `Object X`, where X is a letter. In turn this string is transmitted to the smartphone. The TX is connected, respectively, to a) a fridge, b) mechanical drawers, c) a milling machine and d) an iron clamp. The host PC was offline, as the BCC link requires only a ground connection. We observe that in these experiments some spurious packet reception is possible only with proximity, hence, transmission efficiency is a function of the object conductive surface. In first approximation, the bigger the object, the lower the peak-to-peak voltage required at the TX, and in general, the better. Amplitude control can be implemented by limiting the logic swing of the TX output, using, e.g., an adjustable voltage divider that can be configured once, i.e., when the TX is installed in the furniture that is static.

Fig. 17(b) shows the current consumed by the RX through the battery terminals I_{DD} in an example standard operation

(BT disconnected, BT connected, and during the reception of a PHY packet). The current diagram clearly shows each transition between system states. The average current consumption is 44 mA, resulting in a power consumption of 176 mW (with a measured 4.0 V battery voltage). The TX consumes 100 mW for the transmission shown in Fig. 3. Based on our extensive tests, as expected we have not observed any impact of battery power supply on the performance of the system.

H. Tests on Multiple Subjects
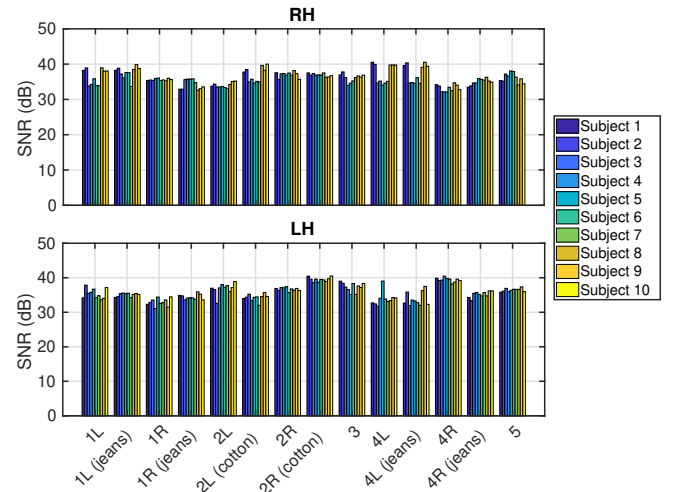
Fig. 18. SNR test on multiple subjects as a function of the RX positioning, left and right hand touch (LH, RH).

We have run tests to verify the correct operation of the device for ten subjects. The tests aimed at establishing both the impact of different bodies and garment on the SNR and verify that the tests on a single subject are confirmed, using the same RX positioning given in Fig. 9(a). Fig. 18 shows the obtained SNR results on the subjects given in

TABLE II

COMPARISON W.R.T. THE STATE-OF-THE-ART

	This Work	[4]	[1]	[43]
TX Mode	Simplex	Full Duplex	Simplex	Full Duplex
TX Electrode	Any	Confined	Confined	Confined
Electrode Size	5.5×3.6 cm (RX)	5×5 cm (bowl)	$\varnothing = 0.4$ cm	3×3 cm$^\natural$
RX to Skin Separation	≤ 2 cm$^\bullet$	Contact/Non-Contact$^\bigcirc$	Contact$^\bigcirc$	Contact$^\bigcirc$
Type	Capacitive	Capacitive	Galvanic	Capacitive
Bit rate	1 kbps*	21.875 kbps	4.8 kbps	1 kbps
Power Supply	3.7 V Li-Po Battery (RX), 5 V (USB), 3.7 V Li-Po Backup (TX)	7.4 V Battery (mobile), 12 V 480 W switching PSU (fixed nodes)	N/A	3.7 V Li-Po Battery (TX) N/A (RX)
TX Output Power (max)	850 nW	<4.95 mW‡	1 mW†	900 nW
TX Output Voltage/Current	2.83 V	5.9 V (min), 9.9 V (max)	± 1 mA on 1 kΩ	10 V
Power Consumption	RX: 176 mW$^\diamond$ (including BT) TX: 100 mW$^\diamond$	N/A	RX: 400 mW TX: 16.5 mW	RX: 525 mW TX (token): 148 mW
Error Rate	~0.1 PER, ~0.25 TER	~0.106 PER (best, 1430 bps)	$< 10^{-4}$ BER (35 cm)	< 0.01 BER

N/A = Not Available. N.a. = Not Applicable. $\diamond$ = Calculated based on the measured 44 mA on a 4.0 V (full charge) battery voltage. $\star$ = Limited by the current software implementation. $\bullet$ = Estimated during normal operation, but dependent on capacitive coupling to ground (signal level proportional to $\frac{C_E C_G}{C_E + C_G}$). $\bigcirc$ = Electrodes on skin with or without direct metal contact, i.e., also when covered by a protective plastics. † = Extracted from TX output current. ‡ = Extracted from the paper (9.9 V and <0.5 mA). $\natural$ = During protection against remote monitoring tests.

Tab. I. During the experiments, the RX electrode is positioned both directly on the subject skin and on the garment, that could be jeans and cotton depending on the specific part of the body. Results shows that garment does not significantly impact on link performance, as the most impacting factor is represented by the RX system distance w.r.t. the body surface. The results do not show a significant variation in the SNR measurement, for a maximum of 8.4 and 9.4 dB in all conditions for RH and LH, respectively. This variability can be attributed to the coupling with the room ground that can vary, even dynamically, between one test and another. However, this ground coupling variation does not significantly impact on system performance as the threshold control can adaptively adjust the comparator level, although with a cycle of delay [assuming a worst case step variation of the conditions, 4 s in the current implementation, see, e.g., Fig. 13(a)]. Once the threshold control loop runs under these lower signal level conditions (and adjusts threshold accordingly), the baseband signal can be still correctly detected. Further measurements in fact, not shown here for the sake of brevity, confirm the TER results obtained for a single subject.

I. Comparison with the State-of-the-Art and Discussion

Tab. II shows a performance comparison of *Live Wire* with respect to the other systems reported in literature. To be consistent, we have included only the most relevant discrete components-based systems, rather than integrated solutions, tightly optimized and achieving extremely low power consumption. Thanks to its inherent low complexity *Live Wire* well suits aggressively optimized integrated circuit implementation: in [7], indeed, a simple envelope detector front-end integrated operating with OOK, 50 kHz center frequency, in a 65 nm technology provides a ~700 pW simulated power consumption. However, besides the front-end part of the receiver, wireless connectivity dominates the power consumption metric, especially due to the requirement of using standard connectivity through portable devices that commonly include BT and Wi-Fi transceivers, rather than ultra-low power solutions such as IR-UWB (here used for ultra-low-power com-

munication rather than localization) [44] that still, are not integrated in commercial portable devices.

Thanks to the low-impedance path to ground of the TX enforced by construction, and the consequent high SNR achievable throughout the body, the system well suits reduced supply voltage (2.83 V v.s. the 5.9 V in [4]). More importantly, the TX can be of any shape in the furniture, therefore with no size limitation. Compared to [45], the system does not require very close electrode-skin distance at the RX, which relaxes wearable requirements. Thanks to its high input impedance, the RX consumes substantially less compared to [43].

VII. CONCLUSIONS

The design of a BCC system based on a non-coherent RX architecture was here reported. The system enables applications in smart infrastructures with increased flexibility compared to ordinary solutions. Results show that to adapt the system usage to diverse objects in the environment, the TX amplitude can be one-time configured once the system installed in the furniture. The system is ready for applicability in experiments with visually impaired people and setups to assess the cognitive improvements that may result both in terms of training and in terms of enhanced perception.

REFERENCES

[1] M. S. Wegmueller, S. Huclova, J. Froehlich, M. Oberle, N. Felber, N. Kuster, and W. Fichtner, "Galvanic Coupling Enabling Wireless Implant Communications," *IEEE Transactions on Instr. and Meas.*, vol. 58, no. 8, pp. 2618–2625, Aug. 2009.

[2] M. S. Wegmueller, M. Oberle, N. Felber, N. Kuster, and W. Fichtner, "Signal Transmission by Galvanic Coupling Through the Human Body," *IEEE Transactions on Instr. and Meas.*, vol. 59, no. 4, pp. 963–969, Apr. 2010.

[3] A. K. Teshome, B. Kibret, and D. Lai, "A Review of Implant Communication Technology in WBAN : Progresses and Challenges," *IEEE Reviews in Biomedical Engineering*, 2018.

[4] V. Varga, G. Vakulya, A. Sample, and T. R. Gross, "Enabling Interactive Infrastructure with Body Channel Communication," *Interactive, Mobile, Wearable and Ubiquitous Technologies*, vol. 1, no. 4, pp. 169–169:29, Dec. 2017.

[5] ——, "Playful Interactions with Body Channel Communication: Conquer it!" in *ACM Symposium on User Interface Software and Technology*, Oct. 2017.

[6] Panasonic Achievements Presented at the Exhibition CEATEC 2016. [Online]. Available: http://www.ceatec.com/2016/news/en-webmagazine/en-005

[7] S. Maity, D. Yang, B. Chatterjee, and S. Sen, "A sub-nW Wake-up Receiver for Human Body Communication," in *IEEE Biomedical Circuits and Systems Conf.*, Oct. 2018, pp. 1–4.

[8] S. Maity, D. Das, B. Chatterjee, and S. Sen, "Characterization and Classification of Human Body Channel as a function of Excitation and Termination Modalities," in *Int. Conf. of the IEEE Engineering in Medicine and Biology Society (EMBC)*, Jul. 2018, pp. 3754–3757.

[9] P. Chanana, R. Paul, M. Balakrishnan, and P. Rao, "Assistive Technology Solutions for Aiding Travel of Pedestrians with Visual Impairment," *Journal of Rehabilitation and Assistive Technologies Engineering*, vol. 4, Jan. 2017.

[10] H. Ka and S. Ravishankar, "Smart Signage: Technology Enhancing Indoor Location Awareness for People with Visual Impairments," 2016. [Online]. Available: http://scholarworks.csun.edu/handle/10211.3/180127

[11] A. R. Jimnez and F. Seco, "Comparing Decawave and Bespoon UWB Location Systems: Indoor/outdoor Performance Analysis," in *IEEE Int. Conf. on Indoor Positioning and Indoor Navigation (IPIN)*, Oct. 2016, pp. 1–8.

[12] T. Grosse-Puppendahl, S. Herber, R. Wimmer, F. Englert, S. Beck, J. von Wilmsdorff, R. Wichert, and A. Kuijper, "Capacitive Near-Field Communication for Ubiquitous Interaction and Perception," Sep. 2014.

[13] Consumer Electronics industry in 2019: Top 5 Trends. [Online]. Available: https://www.eletimes.com/consumer-electronics-industry-in-2019-top-5-trends

[14] M. Crepaldi, G. Zini, A. Maviglia, A. Barcellona, A. Merello, and L. Brayda, "Live Wire: Body Channel Communication as a High Impedance and Frequency-scaled Impulse Radio," in *IEEE Biomedical Circuits and Systems Conf.*, Oct. 2017, pp. 1–4.

[15] J. Zhao, J. Mao, T. Zhou, L. Lai, H. Yang, and B. Zhao, "An Auto Loss Compensation System for Non-contact Capacitive Coupled Body Channel Communication," in *IEEE Int. Symposium on Circuits and Systems*, May 2018, pp. 1–5.

[16] J. Mao, B. Zhao, Y. Lian, and H. Yang, "A Self-adaptive Body Channel Communication Scheme for Backward Path Loss Reduction," in *IEEE Int. Symposium on Circuits and Systems*, May 2016, pp. 2034–2037.

[17] J. Bae and H. Yoo, "The Effects of Electrode Configuration on Body Channel Communication Based on Analysis of Vertical and Horizontal Electric Dipoles," *IEEE Transactions on Microwave Theory and Techniques*, vol. 63, no. 4, pp. 1409–1420, Apr. 2015.

[18] P. Tsai, Y. Chang, S. Hsu, and C. Lee, "An OFDM-based 29.1Mbps 0.22nJ/bit Body Channel Communication Baseband Transceiver," in *VLSI Design, Automation and Test*, Apr. 2015, pp. 1–4.

[19] MicroPython. [Online]. Available: https://micropython.org/

[20] M. Khamphroo, N. Kwankeo, K. Kaemarungsi, and K. Fukawa, "MicroPython-based Educational Mobile Robot for Computer Coding Learning," in *Int. Conf. of Information and Communication Technology for Embedded Systems*, May 2017, pp. 1–6.

[21] MicroPython May Be Powering Your Next Embedded Device. [Online]. Available: https://www.designnews.com/electronics-test/micropython-may-be-powering-your-next-embedded-device/164173310860457

[22] M. Brambring, "Mobility and Orientation Processes of the Blind," in *Electronic Spatial Sensing for the Blind*, 1985, pp. 493–508.

[23] W. Ugulino and H. Fuks, "Landmark Identification with Wearables for Supporting Spatial Awareness by Blind Persons," in *ACM Int. Joint Conf. on Pervasive and Ubiquitous Computing*, Sept. 2015.

[24] A. K. Ganguli, D. Pushp, and A. Chaudhary, "Electronic Travel Aids ETA for Blind Assistance–A Review," *Int. Journal of Engineering Science and Computing*, vol. 6, no. 3, pp. 2672–2675, Mar. 2016.

[25] G. Kleege, "Visible Braille/Invisible Blindness," *Journal of Visual Culture*, vol. 5, no. 2, pp. 209–218, Aug. 2006.

[26] (2011–2014, Jun.) An1391: Introduction to the bodycom technology. [Online]. Available: ww1.microchip.com/downloads/en/AppNotes/00001391C.pdf

[27] P. N. Whatmough, G. Smart, S. Das, Y. Andreopoulos, and D. M. Bull, "A 0.6V All-Digital Body-Coupled Wakeup Transceiver for IoT Applications," in *Symposium on VLSI Circuits (VLSI Circuits)*, Jun. 2015, pp. C98–C99.

[28] J. Jang, H. Cho, and H. Yoo, "An 802.15.6 HBC Standard Compatible Transceiver and 90 pJ/b Full-Duplex Transceiver for Body Channel Communication," in *IEEE Biomedical Circuits and Systems Conf.*, Oct. 2019, pp. 1–4.

[29] Christiane Attig and Nadine Rauh and Thomas Franke and Josef F. Krems, "System Latency Guidelines Then and Now – Is Zero Latency Really Considered Necessary?" in *HCI*, 2017.

[30] J. Huang, L. Wang, D. Zhang, and Y. Zhang, "A Low-frequency Low-noise Transceiver for Human Body Channel Communication," in *IEEE Biomedical Circuits and Systems Conf.*, Nov. 2009, pp. 37–40.

[31] H. Cho, H. Kim, M. Kim, J. Jang, Y. Lee, K. J. Lee, J. Bae, and H. Yoo, "A 79 pJ/b 80 Mb/s Full-Duplex Transceiver and a 42.5μW 100 kb/s Super-Regenerative Transceiver for Body Channel Communication," *IEEE Journal of Solid-State Circuits*, vol. 51, no. 1, pp. 310–317, Jan. 2016.

[32] H. Cho, J. Bae, and H. Yoo, "A 39 μW Body Channel Communication Wake-up Receiver with Injection-locking Ring-oscillator for Wireless Body Area Network," in *IEEE Int. Symposium on Circuits and Systems*, May 2012, pp. 2641–2644.

[33] H. Cho, H. Kim, M. Kim, J. Jang, Y. Lee, K. J. Lee, J. Bae, and H. Yoo, "A 79 pJ/b 80 Mb/s Full-Duplex Transceiver and a 42.5μW 100kb/s Super-Regenerative Transceiver for Body Channel Communication," *IEEE Journal of Solid-State Circuits*, vol. 51, no. 1, pp. 310–317, Jan. 2016.

[34] M. A. Hannan, S. M. Abbas, S. A. Samad, and A. Hussain, "Modulation Techniques for Biomedical Implanted Devices and Their Challenges," *Sensors (Basels)*, vol. 1, no. 12, pp. 297–319, Dec. 2012.

[35] M. Crepaldi and P. Kinget, "Error Ratio Model for Synchronised-OOK IR-UWB Receivers in AWGN Channels," *Electronics Letters*, vol. 49, no. 1, pp. 25–27, Jan. 2013.

[36] S. Vijayalakshmi and V. Nagarajan, "Energy efficient low density parity check scheme for body channel communication using FPGA," *Microprocessors and Microsystems*, vol. 68, pp. 84 – 91, 2019.

[37] J. Hwang, T. Kang, J. Kwon, and S. Park, "Effect of Electromagnetic Interference on Human Body Communication," *IEEE Transactions on Electromagnetic Compatibility*, vol. 59, no. 1, pp. 48–57, Feb. 2017.

[38] X. Ling, B. Wu, H. Wen, P. Ho, Z. Bao, and L. Pan, "Adaptive Threshold Control for Energy Detection Based Spectrum Sensing in Cognitive Radios," *IEEE Wireless Communications Letters*, vol. 1, no. 5, pp. 448–451, Oct. 2012.

[39] MicroPython Documentation – Release 1.9.2. [Online]. Available: https://media.readthedocs.org/pdf/micropython/latest/micropython.pdf

[40] Zecheng Xie, Rongtao Xu, and Lei Lei, "A Study of Clear Channel Assessment Performance for Low Power Wide Area Networks," in *Int. Conf. on Wireless Communications, Networking and Mobile Computing*, Sep. 2014, pp. 311–315.

[41] Bluetooth Smart Software API Reference Manual. [Online]. Available: https://www.silabs.com/documents/login/reference-manuals/bluetooth-api-reference-261.pdf

[42] "Guidelines for Limiting Exposure to Time-Varying Electric, Magnetic, and Electromagnetic Fields (up to 300 GHz)," in *Health Physics*, 1998, pp. 494–522.

[43] V. Nguyen, M. Ibrahim, H. Truong, P. Nguyen, M. Gruteser, R. Howard, and T. Vu, "Body-Guided Communications: A Low-power, Highly-Confined Primitive to Track and Secure Every Touch," in *Int. Conf. on Mobile Computing and Networking*, 2018, pp. 353–368.

[44] R. Liu, B. R. Carlton, S. Pellerano, F. Sheikh, D. S. Vemparala, A. Ali, and V. S. Somayazulu, "A 264-μW 802.15.4a-Compliant IR-UWB Transmitter in 22nm FinFET for Wireless Sensor Network Application," in *IEEE Radio Frequency Integrated Circuits Symposium (RFIC)*, Jun. 2018, pp. 164–167.

[45] M. S. Wegmueller, W. Fichtner, M. Oberle, and N. Kuster, "BPSK & QPSK Modulated Data Communication for Biomedical Monitoring Sensor Network," in *IEEE Int. Conf. of the Engineering in Medicine and Biology Society*, Aug. 2006, pp. 2071–2074.
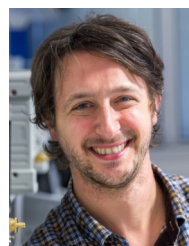
Marco Crepaldi (M'9) received the engineering degree (summa cum laude) and the Ph.D. in electronic engineering from the Politecnico di Torino (Polito), Turin, Italy, in 2005 and 2009, respectively. During 2008 he was a Visiting Scholar at the Electrical Engineering Department of Columbia University in the City of New York. After the Ph.D., he worked as a Postdoc at the VLSI-Lab, Electrical Engineering department, PoliTo, and then as a Postdoc at the former Istituto Italiano di Tecnologia@PoliTo Center for Space Human Robotics (IIT-CSHR). He is now the coordinator of the Electronics Design Lab (edl.iit.it) at the IIT Center for Human Technology in Genova. His scientific activity is related to the analysis, simulation and development of integrated event-driven and all-digital Impulse-Radio Ultra-Wide Band (IR-UWB) systems. He is author and co-author of more than 60 publications and two international patents.

Alessandro Barcellona received the engineering degree (summa cum laude) in automation engineering from University of Palermo in 2007. He obtained a research grant in Biophysics field at the National Research Council (CNR) of Palermo for the hardware and software design of the instrumentation electronic control and command for Atomic Force Microscopy (AFM) on living cells. He joined the Nanophysics department of the Istituto Italiano di Tecnologia (IIT) and his main activities regarded the hardware and software design and implementation of electronic devices for open source and automated microscopy imaging systems. He is now a technician of the Electronic Design Lab (edl.iit.it) facility. His main activities regard hardware design, short-term electrical & physical design, reworking and assembly management.

Giorgio Zini received the high school diploma in 1978 (Liceo Scientifico L. Respighi in Piacenza) and developed a deep knowledge in electronic design and R&D management working (since 1979) as employee in several companies (Computer Application Engineering and Silverstar ltd. in Milan, Ansaldo S.p.A., Esacontrol and Orsi Automazione s.r.l. in Genova, Rubbini s.r.l. in Bologna) and also as a member of a R&D company (LUZ elettronica in Piacenza). He worked as a consultant for prestigious firms and organizations like Siemens S.p.A., DESY Accelerator Consortium, British Petroleum, Enel, Ferrovie Italiane and Università di Genova. Now he is Senior Electronic Designer in Electronic Design Laboratory (EDL) of the Istituto Italiano di Tecnologia (IIT, Genova). His experience covers many fields in electronic engineering: microprocessor and embedded microcontroller systems, analog data acquisition systems, digital signal processors, FPGA and CPLD devices, high speed data transmission in local area and wide area networks, switched mode power supplies, PWM motor controllers, very-low power battery operated and solar-cells powered devices. During his 39 year career Mr. Zini successfully designed (or participated in the development of) hundreds of electronic systems ranging from small pocket devices, to large industrial plants.

Alberto Ansaldo holds a MSc in Electronics Engineering and a Ph.D. in Communication Science and Technology focused on chemical vapor deposition of carbon nanotubes for electronic applications. He joined the Italian Institute of Technology in 2008 as a founder of the Soft Materials Design Laboratory, mainly working in carbon nanomaterial composite applications in robotics and neuroprosthetics. In 2015, he joined the IIT Graphene Labs. His current research interests encompass 2D crystals production and applications, with a focus on supercapacitors and Li-ion batteries. He is currently an R&D specialist at ASG Superconductors. He is author of more then 70 publications and 8 granted patents.

Paolo Motto Ros is Senior Post-Doc Researcher at Politecnico di Torino (Torino, Italy), Dipartimento di Elettronica e Telecomunicazioni, with the MiNES (Micro&Nano Electronic Systems) group. He received the electronic engineering degree and the Ph.D. in electronic engineering from the Politecnico di Torino, Torino, Italy, in 2005 and 2009, respectively. From 2009 to 2012 he was with Neuronica Laboratory (Dipartimento di Elettronica, Politecnico di Torino) as post-doc researcher, jointly with, 2006-2011, Istituto Nazionale Fisica Nucleare, INFN, Italy. From 2012 to 2019 he was with Istituto Italiano di Tecnologia (Center for Space Human Robotics, CSHR, Torino, Italy, and, since 2016, Electronic Design Laboratory, EDL, Genova, Italy) as senior (since 2014) post-doc researcher. He joined the Politecnico di Torino, Dipartimento di Elettronica e Telecomunicazioni, in 2019. He is an IEEE member since 2016, and member of the Circuits And Systems (CAS) society; he was member of the organizing staff of the IEEE BioCAS 2017 conference, and member of the organizing committee of the IEEE ICECS 2019 conference. He counts >40 publications; current research interests include: event-driven digital integrated circuits, architectures, and systems; low-power smart sensor networks; bio-inspired electronics; biomedical and humanoid robotic applications.

Alessandro Sanginario received the masters degree in biomedical engineering and the Ph.D. degree in physics from the Politecnico di Torino, in 2006 and 2011, respectively. From 2006 to 2007, he was with the Chilab Material and Microsystems Laboratory, Politecnico di Torino. He was a Visiting Ph.D. Student with the Vestfold University College, Norway, during his Ph.D. period. From 2012 to 2017, he held a Post-Doctoral position at the Center for Space Human Robotics, with the Italian Institute of Technology. He is now research technician with Electronics Dept. of Politecnico di Torino. His research interests concern microelectromechanical systems and advanced sensors, in particular, for biomedical applications.

Claudia Cuccu received Bachelors degree in Biomedical Engineering at University of Cagliari in 2016 and received Masters degree in Biomedical Engineering with major in Biomedical instrumentation at Politecnico di Torino in October 2019, discussing a thesis entitled: "Modeling and characterization of a body channel communication system". Main research interests are Biomedical Signal Processing, Body channel communication, and Bionanotechnologies.

Danilo Demarchi (M10-SM13) received Engineering Degree and Ph.D. in Electronics Engineering from Politecnico di Torino, Italy, in 1991 and 1995, respectively. Full position as Associate Professor at Politecnico di Torino, Department of Electronics and Telecommunications. Visiting Professor at EPFL Lausanne and at Tel Aviv University. Visiting Scientist (August 2018) at MIT and Harvard Medical School. Author and co-author of 3 patents and more than 200 scientific publications in international journals and peer-reviewed conference proceedings. Leading the MiNES (Micro&Nano Electronic Systems, http://mines.polito.it) Laboratory of Politecnico di Torino. Member of the BioCAS Technical Committee, Associate Editor of the Transactions on Biomedical Circuits and Systems (TBioCAS), of the Open Journal of Engineering in Medicine and Biology (OJ-EMB), of IEEE Sensors and of the Springer-Nature Journal BioNanoScience. General Chair of BioCAS 2017 (Biomedical Circuits and Systems) and founder of IEEE FoodCAS Workshop (Circuits and Systems for the Food Chain).

Luca Brayda obtained his MSc in Computer Science Engineering at Politecnico di Torino in 2003, with a Master Thesis at the Panasonic Speech Technology lab of Santa Barbara, USA, supervised by Jean-Claude Junqua and Luca Rigazio. In 2007 he got his PhD from the University of Nice-Sophia Antipolis, France, supervised by Christian Wellekens and Maurizio Omologo. His research on microphone arrays for robust speech recognition was hosted by the Eurecom Institute, France and by the Fondazione Bruno Kessler, Trento, Italy. From 2008 he is Team Leader at the Italian Institute of Technology, in the Robotics, Brain and Cognitive Sciences dept., headed by Giulio Sandini. He has worked in multimedia communications, telerobotics and virtual environments. His current interests are on haptics, acoustics and audio augmented reality, with applications in assistive technologies to compensate sensory impairment and augment human capabilities. He was coordinator of the European FP7 STREP 2014-2017 project BLINDPAD (www.blindpad.eu). He is author of more than 30 international publications and 2 international patents.

RESPONSES TO REVIEWERS' COMMENTS

AE COMMENTS

The authors have satisfactorily addressed many of the most important issues raised by the reviewers. However, the manuscript still has some deficiencies with respect to language use. Several typos and language problems remain throughout the revised submission. The authors should have the paper carefully proofread and revised before resubmission.

Thank you again for having coordinated the review of our paper and for having brought to us these important points. We have now carefully re-checked the complete manuscript sentence by sentence and adjusted these English mistakes. We have also checked the manuscript for other errors (e.g., figures numbering) and corrected them.

In addition, in the new experimental results with multiple subjects, it is unclear what would be the overall impact of a 9.4dB variability in the overall functionality of the device. The authors are encouraged to include a brief discussion in that regard.

Thanks for the suggestion. We have now briefly discussed this impact on L910-920.

REVIEWER 1

This paper is a revision of an earlier submission and describes a body-channel-communication (BCC) system. My first review raised a number of issues. These issues have been addressed by removing some content, adding an additional evaluatoin, and enlarging the description of the (low-level) PHY protocol/implementation.

Thank you again for the helpful suggestions. We think that your suggestions helped us improving a lot our manuscript.

One of the strong points of the first version was that it introduced an interesting application scenario. The current version has reduced this part to just briefly mention this problem domain. In the end, this decision of the authors should be applauded, as the evidence to support the use of this BCC implementation to assist visually-impaired person was weak.

Thank you again for the suggestion.

As a result of these changes, the main topic of the paper is the low-level hardware and software of a PHY layer for BCC. This part is difficult to read (see language comments below) and – maybe – of moderate interest to the readers of this journal.

We have now tried to process the manuscript and carefully proof-read it to eliminate English mistakes and correct other reference mistakes we have found (e.g., figure numbering).

Some of the figures are impossible to read without substantial magnification (e.g., Fig 7; only at 400x can the labels be read). Or the figures are confusing (e.g., Fig 13 with different scales on the x-axis of (a), (b), and (c), as well as different ranges for these three sub-figures). Is there any reason to show these three figures aligned in one figure?

The reason to show these three sub-figures aligned vertically is to optimize space not to increase paper length, and at the same time maintain readability. The different x-axis spans are related directly to the phenomena we wanted to observe, and they are not necessarily equal. However, we have decided to uniform the x-axes for all figures with a 60 s span.

Moreover, since it was not readable enough, we have now increased font size of Fig. 6, as well.

In the discussion of Modulation and Signaling, N_w is introduced as "Each symbol comprises a square wave of N_w periods", but it's shown in Fig. 3 as a time interval. And are these pulses really part of T_s0 as Fig. 3 suggests?

Thanks for pointing this out. Indeed the correct indication is $N_\mathrm{w}T_\mathrm{p}$ because the indicated label must have time units. We have now corrected the figure and added a note on L279-280 to make clearer.

The x-axis and the y-axis of Fig. 14 have no labels.

Please consider that the x and y-labels in the figure are specified in the center of the figure below the human body silhouette. These labels apply to all axes in the figure. We have modified the caption of the figure to make clearer.

Furthermore, even in its current form, the paper contains many English language issues (e.g., subject verb agreement, wrong word – "variegated environmental objects" [color was never discussed before], "The literature is disseminated with Electronic Travel Aids (ETA)" [maybe populated? filled with?]).

Thanks for the suggestion. We have now reprocessed to manuscript to improve the English form.

REVIEWER 2

The revised paper R1 addressed most of my comments and suggestions. It reads better now, though with an effort because it was edited in MS Word and it kept a lot of strikethrough text...

Thank you for having reviewed again our paper. We are sorry if the font encoding does not look well but we are using the IEEE tran Latex package, combined with Latexdiff to enlighten text additions and removals. Maybe you are referring to the difference file and not to the full manuscript. We had submitted them both on the TETC site. This was the default font that was implemented in the Latex package. We have deiced not to change this not to impact on page length, therefore making it difficult to the reviewers to check if the length of the manuscript exceeds the specifications of the journal.